Research Article

Check for updates

Lycium barbarum polysaccharides ameliorate canine acute liver injury by reducing oxidative stress, protecting mitochondrial function, and regulating metabolic pathways

Jianjia HUANG[1,2], Yuman BAI[1], Wenting XIE[1], Rongmei WANG[3], Wenyue QIU[1], Shuilian ZHOU[1], Zhaoxin TANG[1], Jianzhao LIAO[1], Rongsheng SU[1✉]

[1]*College of Veterinary Medicine, South China Agricultural University, Guangzhou 510642, China*
[2]*Guangzhou General Pharmaceutical Research Institute Co., Ltd., Guangzhou 510240, China*
[3]*College of Biology and Agriculture, Shaoguan University, Shaoguan 512005, China*

Abstract: The development of acute liver injury can result in liver cirrhosis, liver failure, and even liver cancer, yet there is currently no effective therapy for it. The purpose of this study was to investigate the protective effect and therapeutic mechanism of *Lycium barbarum* polysaccharides (LBPs) on acute liver injury induced by carbon tetrachloride (CCl_4). To create a model of acute liver injury, experimental canines received an intraperitoneal injection of 1 mL/kg of CCl_4 solution. The experimental canines in the therapy group were then fed LBPs (20 mg/kg). CCl_4-induced liver structural damage, excessive fibrosis, and reduced mitochondrial density were all improved by LBPs, according to microstructure data. By suppressing Kelch-like epichlorohydrin (ECH)-associated protein 1 (Keap1), promoting the production of sequestosome 1 (SQSTM1)/p62, nuclear factor erythroid 2-related factor 2 (Nrf2), and phase II detoxification genes and proteins downstream of Nrf2, and restoring the activity of anti-oxidant enzymes like catalase (CAT), LBPs can restore and increase the antioxidant capacity of liver. To lessen mitochondrial damage, LBPs can also enhance mitochondrial respiration, raise tissue adenosine triphosphate (ATP) levels, and reactivate the respiratory chain complexes I–V. According to serum metabolomics, the therapeutic impact of LBPs on acute liver damage is accomplished mostly by controlling the pathways to lipid metabolism. 9-Hydroxyoctadecadienoic acid (9-HODE), lysophosphatidylcholine (LysoPC/LPC), and phosphatidylethanolamine (PE) may be potential indicators of acute liver injury. This study confirmed that LBPs, an effective hepatoprotective drug, may cure acute liver injury by lowering oxidative stress, repairing mitochondrial damage, and regulating metabolic pathways.

Key words: Acute liver injury; Oxidative stress; Mitochondrial dysfunction; Metabolomics; *Lycium barbarum* polysaccharides

1 Introduction

Liver illness has emerged as a major worldwide health issue, particularly acute liver injury which is associated with a high death rate (Wu et al., 2010). The acute liver injury model induced by carbon tetrachloride (CCl_4) is widely used to investigate potential treatment strategies and find markers for evaluating liver injury (Zhang et al., 2014; Guo et al., 2017).

✉ Rongsheng SU, srsh168@163.com

Rongsheng SU, https://orcid.org/0000-0003-4574-5076
Jianjia HUANG, https://orcid.org/0000-0002-0685-3237

Natural substances extracted from plants have been investigated as a reliable and safe method for treating liver disease in recent years. *Lycium barbarum* polysaccharides (LBPs) are a water-soluble glycoconjugate composed of seven monosaccharides isolated from the *L. barbarum* berries. The fundamental cause of the substantial pharmacological action of *L. barbarum* berries is thought to be LBPs, which comprise the principal bioactive component of the berries (Du et al., 2022). LBPs have attracted wide attention because of their potential health promotion. LBPs have pharmacological actions that include anti-tumor, immune system modulation, apoptosis inhibition, DNA damage reduction, and neuroprotection (Tian et al., 2019). However, the therapeutic impact of LBPs and their precise mechanism

of action with regard to acute liver injury are still up for debate.

Kelch-like epichlorohydrin-associated protein 1 (Keap1)-nuclear factor erythroid 2-related factor 2 (Nrf2)-antioxidant response elements (AREs), one of the most significant cell defense systems, is crucial for preserving redox homeostasis in the liver (Jia et al., 2019). AREs with cytoprotective effect, such as super-oxide dismutases (SOD1, SOD2), thioredoxins (Trx1, Trx2), heme oxygenase-1 (HO-1), catalase (CAT), glutathione reductase (GR), glutathione peroxidases (GPX1, GPX4), glucose-6-phosphate dehydrogenase (G6PD), and peroxiredoxin 3 (PRDX3), are regulated by Nrf2. Additionally, Nrf2 controls the synthesis and transcription of various drug metabolic enzymes (DMEs), transporters and cellular reduction equiva-lents such as glutathione (GSH) and nicotinamide ade-nine dinucleotide phosphate (NADPH), as well as re-active oxygen inactivating enzymes, which together form an Nrf2-dependent antioxidant defense system (Ma, 2010; Chen et al., 2020). Another protein, p62, also known as sequestosome 1 (SQSTM1), has been identified, which can activate Nrf2 by inactivating Keap1 (Zhao et al., 2021). When autophagy activity is impaired or oxidative stress damage occurs, p62 binds to Keap1 and transports it to autophagosomes for degradation, promoting the activation of Nrf2 and downstream AREs (Bellezza et al., 2018). It is important to note that since AREs happen to be included in the promoter of p62, p62 is also the transcriptional target of Nrf2 (Jain et al., 2010).

Reactive oxygen species (ROS) are overproduced and released into the cytoplasm when mitochondrial function is compromised. Oxidative phosphorylation (OXPHOS) is hindered, the supply of adenosine tri-phosphate (ATP) is decreased, and these events all occur simultaneously. DNA, proteins, and lipids are then oxidized, leading to cell death (Lustgarten et al., 2012; Jardim et al., 2020). The progression of CCl_4-induced acute liver injury depends heavily on mito-chondrial dysfunction (Lin et al., 2019). Changes in cell metabolites are crucial for tissue homeostasis and regeneration, and can also be used as an indicator of liver illness (Caldez et al., 2018). Metabolomics is often used to obtain a thorough grasp of the causes of various physiological states and aberrant processes since it is a technique for identifying small alterations in biological metabolic pathways (Johnson et al., 2016).

The information obtained by metabolomics is closer to the meaningful pathological or physiological pheno-type, but no metabolomic investigations of the thera-peutic impact of LBPs on canine acute liver injury have been published.

To sum up, the aim of this study was to confirm the therapeutic action of LBPs, clarify the therapeutic mechanism of LBPs on acute liver injury through oxi-dative stress, mitochondrial function, and metabolic pathways, and provide theoretical support and refer-ences for the future clinical application of LBPs.

2 Materials and methods

2.1 Animals

At the experimental animal base in South China Agricultural University, a total of 18 healthy mongrel canines (half females, half males), ranging in age from one to two years, were reared under the stan-dard conditions of constant temperature ((25±2) °C). The kennel was fully cleansed and disinfected be-fore the experiment, and all canines were reared ad-aptatively for a week, with unlimited access to food and water. All canines were found to be healthy be-fore the trial based on physical, blood routine, and blood chemistry examinations.

2.2 Experimental procedure

The 18 mongrel canines were randomly divided into three groups: control group (CG), model group (MG), and treatment group (TG). There were six ca-nines in each group (three females and three males). Autoclaved peanut oil was combined at 1:1 volume ratio with CCl_4 (C805332, Macklin, Shanghai, China) on the first day of the experiment. The canines in the MG and TG were intraperitoneally injected with CCl_4 plus peanut oil at a dosage of 1 mL/kg to provide a model of acute liver injury, while the CG was injected with peanut oil at the same dose. To assess whether the development of the acute liver injury model was effective or not, the blood levels of aspartate amino-transferase (AST) and alanine aminotransferase (ALT) were measured 24 h later using an automated bio-chemical analyzer (BS380, Mindray, Shenzhen, China). LBPs (20 mg/kg, this dose refers to the previous description by Xin et al. (2011) (SP9310, Solarbio, Beijing, China) were dissolved and combined with the

necessary amount of distilled water, and the canines in the TG were fed once daily for 14 consecutive days after the model had been established (Fig. S1). After 14 d, all canines were anesthetized by pentobarbital sodium and euthanized, and blood and liver tissue samples were collected for further analysis. Every 3 d, all canines were weighed to ensure accurate dosage and to record statistics.

2.3 Histopathological observations

After fixing the liver tissue with 4% (volume fraction) paraformaldehyde for more than 48 h, the liver tissue was dehydrated with 50%, 70%, 80%, 90%, and 100% (volume fraction) alcohol, respectively, and then embedded in paraffin. The embedded liver tissue was cut into 4-μm-thick slices by a slicer and fixed on a glass slide treated with 3-aminopropyltriethoxysilane (APE), then stained with hematoxylin and eosin (H&E), and finally observed with an optical microscope (DM1000, Leica, Wetzlar, Germany).

2.4 Western blot analysis

The expression of oxidative stress-related proteins was detected by western blotting, carried out according to Liu BX et al. (2021) (supplementary materials and methods). The main antibodies used in this experiment were: p62 (1:2000 (volume ratio, the same below), PA5-27247, Thermo Fisher, Waltham, USA), Keap1 (1:2000, bs-3648R, Bioss, Beijing, China), Nrf2 (1:1000, bs-1074R, Bioss), HO-1 (1:2000, ab52947, Abcam, Cambridge, USA), Trx1 (1:1000, ab109385, Abcam), SOD1 (1:1000, ab13498, Abcam), GPX4 (1:2000, BS7323, Biogot, Nanjing, China), 8-hydroxy-2-deoxyguanosine (8-OHDG) (1:100000, NB600-1508, Novus, Littleton, USA), glyceraldehyde-3-phosphate dehydrogenase (GAPDH) (1:10000, AP0063, Biogot), β-actin (1:10000, AP0060, Biogot), and histone H3 (1:2000, T56587, Abmart, Shanghai, China).

2.5 qPCR

Quantitative real-time polymerase chain reaction (qPCR) was used to detect the expression levels of genes, as described previously (Liu BX et al., 2021) Detailed procedures are included in the supplementary materials and methods. The sequences of relevant primers for qPCR analysis in this experiment are shown in Table S1.

2.6 Immunohistochemistry

The expression levels and localizations of p62, Nrf2, and 4-hydroxynonenal (4-HNE) proteins in cells were detected by immunohistochemistry (supplementary materials and methods).

2.7 Masson staining

A modified Masson Trichromatic Staining kit (G1346, Solarbio) was used to evaluate the extent of liver fibrosis in accordance with the manufacturer's instructions (supplementary materials and methods). The degree of liver fibrosis in each experimental group was assessed in accordance with the collagen fiber area ratio after comparing the collagen fiber area with the total tissue area.

2.8 Electron microscopic observation

The liver tissues of specimens trimmed to 1 mm× 1 mm×1 mm specification were fixed with 2.5% (volume fraction) glutaraldehyde (pH=7.4, 4 °C) for 24 h, diluted overnight with phosphate-buffered saline (PBS) at 4 °C, and then fixed in 1% (volume fraction) samarium tetroxide, dehydrated with ethanol, and finally embedded in epoxy resin. The tissue blocks were trimmed and sliced into 80-nm slices with a slicing machine. The ultrastructure was observed with a transmission electron microscope (TEM; H-7500, Hitachi, Tokyo, Japan).

2.9 Determination of parameters related to oxidative damage

The liver tissue stored at −80 °C was thawed, reagent was prepared in advance according to the manufacturer's instructions, and an appropriate amount of tissue was taken to operate on the ice. The G6PD, thioredoxin reductase (TrxR) enzyme activity, hydrogen peroxide (H_2O_2) content (BC1155, BC3595, Solarbio), the CAT, SOD1, SOD2, GPX, GR enzyme activity, and GSH and malondialdehyde (MDA) content (S0051, S0103, S0058, S0055, S0053, S0131S, Beyotime, Shanghai, China) were measured correctly. All the operations in the experiment were carried out in accordance with the kit instructions.

2.10 Determination of parameters related to mitochondrial function

The liver tissue (0.1 g) was weighed precisely. The ATP content was ascertained in accordance with

the conditions, procedures, and instructions of the ATP Content Detection Kit (BC0305, Solarbio).

The mitochondria of the liver tissue were extracted using the standard steps of differential centrifugation and at 4 °C (Venâncio et al., 2013). The isolated mitochondria were lysed before the bicinchoninic acid (BCA) protein concentration determination kit was used to measure the concentration of mitochondrial protein, and diluted to an appropriate level. Spectrophotometry was then used to assess the respiratory chain complexes I–V activity in the isolated mitochondria in accordance with a published method (Wang et al., 2017). Citrate synthase (CS) activity was used to adjust the measured complexes I–V activity for the potential presence of variable amounts of non-mitochondrial protein in various mitochondrial preparations, which was assessed as previously mentioned (Frazier et al., 2020).

The mitochondrial respiration rate of liver tissue was assessed at room temperature using a mitochondrial respirometer (Oxygraph-2k, Oroboros, Innsbruck, Austria). A total of 10 mg of fresh liver tissue was placed in respiratory medium and ground with a tissue grinder. The mixture was then added to the chamber of the respiratory apparatus to measure the basic oxygen consumption rate of mitochondria and the steady-state oxygen flux obtained by adding specific substrates: 10 mmol/L glutamic acid and 2 mmol/L malic acid were used to evaluate complex I, and 10 µmol/L cytochrome C was used to verify the integrity of liver cell membranes. Totally, 4 mmol/L adenosine diphosphate (ADP) was used to evaluate the phosphorylation process of synthetic ATP. The maximum uncoupling of mitochondria could be obtained by titrating 2 µmol/L carbonyl cyanide 4-trifluoromethoxy-phenylhydrazone (FCCP), and then 0.5 µmol/L rotenone (complex I inhibitor) and 2.5 µmol/L antimycin A (complex III inhibitor) were added to completely inhibit respiration. Finally, the data were derived and analyzed by DatLab7 software.

2.11 Non-targeted metabolomics detection

The main process and data analysis were as previously described (Qiao et al., 2021). Detailed procedures are included in the supplementary materials and methods. The selected metabolites were analyzed by multivariate statistical analysis with SIMCA 14.1 (Figs. S2–S7).

2.12 Statistical analysis

The results are expressed as mean±standard deviation (SD). GraphPad Prism 7.0 (https://www.graphpad.com/scientific-software/prism) was used for statistical analysis and image drawing, while Student's *t*-test was used to evaluate whether there were significant differences between the two groups. The metabolites were screened and analyzed by SIMCA 14.1. The Human Metabolome Database (HMDB; http://www.hmdb.ca) was used to identify metabolites, Kyoto Encyclopedia of Genes and Genomes (KEGG; http://www.genome.jp/kegg) analysis was used to find metabolic pathways, and MetaboAnalyst 5.0 (http://www.metaboanalyst.ca) was used to enrich pathways and construct heat maps.

3 Results

3.1 Reduction of the liver dysfunction and pathological injury of CCl$_4$-induced acute liver injury by LBPs

On the days following CCl$_4$ injection, canine ALT and AST levels in the MG and TG were considerably higher than those in the CG (Fig. 1a). The blood AST and ALT levels of the MG had dropped, but were still high on Day 14 after the model was formed and stable. In contrast, those in the TG were significantly lower than those in the MG (*P*<0.01), and the serum AST levels of the TG had reverted to the normal range.

Fig. 1b depicts abnormal alterations to the liver tissue. Compared to the CG, the hepatic tissue in the MG showed a significant area of fragmented necrosis, virtually no liver cord structure, hepatocytes with abnormal morphology and fatty degeneration, nuclear pyknosis and dissolution, dilated and clogged hepatic sinuses, and a significant amount of hemoglobin being broken down and converted into hemosiderin adhesion. Although the hepatic cord structure of the TG was obvious and cell morphology was complete, there were still some incomplete hepatocytes with steatosis and congested hepatic sinusoids.

The liver ultrastructure is shown in Fig. 1c. The density of mitochondria in the MG was substantially lower than that in the CG (there were few mitochondria in a single hepatocyte), and there was vacuolation within the mitochondria as well as partial nuclei that were distorted and cleaved as the nucleolus disintegrated and vanished. Unlike in the MG, the density
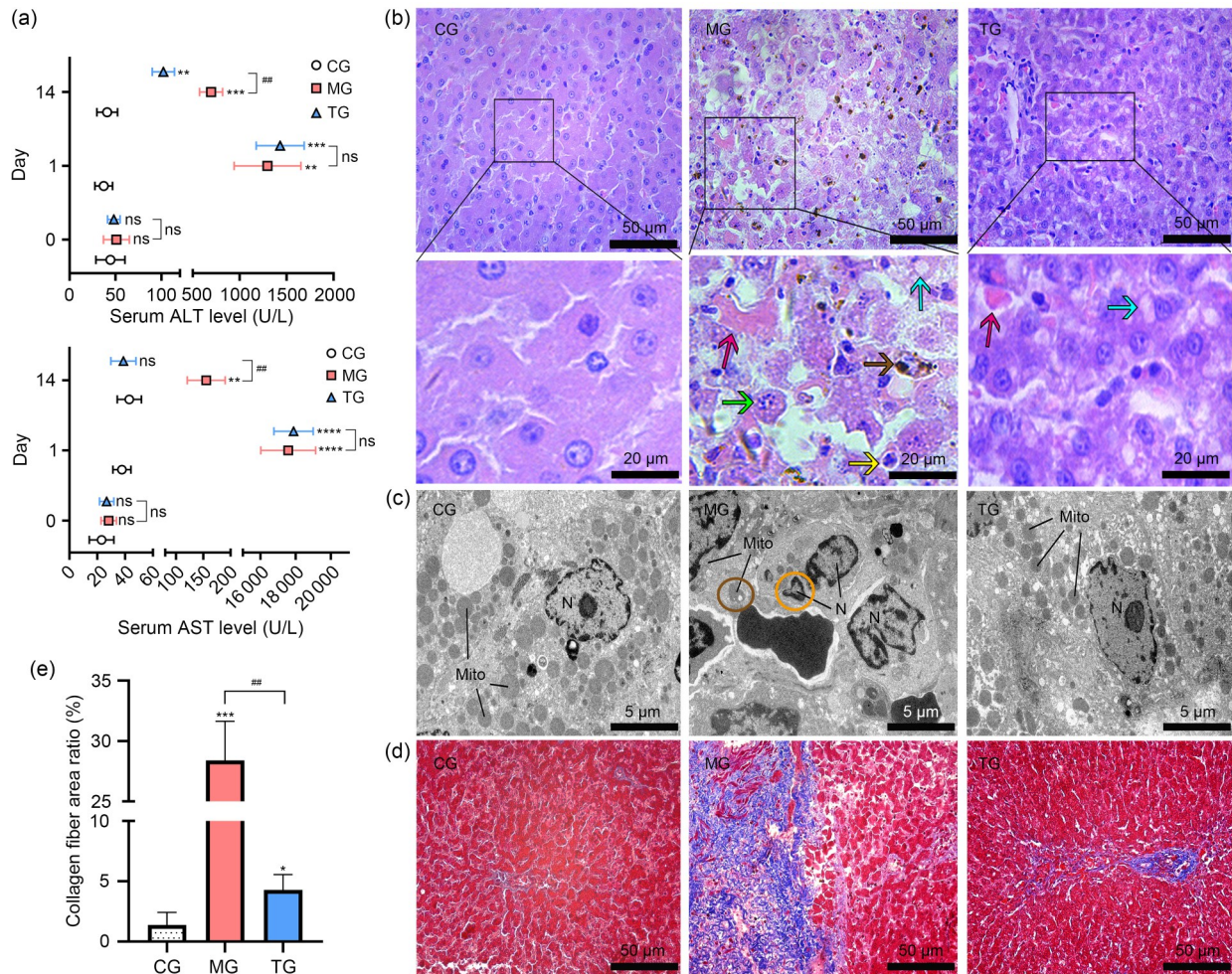
Fig. 1 Protective effect of LBPs on acute liver injury induced by CCl₄. (a) The levels of serum ALT and AST in the three groups. (b) The H&E staining result: the red arrow refers to hepatic sinusoid congestion; the green arrow refers to nucleus dissolution; the yellow arrow refers to nucleus pyknosis; the brown arrow refers to hemosiderin deposition; and the blue-green arrow refers to steatosis. (c) Ultrastructural display of hepatocytes. Mito: mitochondria; N: nucleus; Brown circle: vacuolated mitochondria; Orange circle: nuclear debris. (d, e) The results of Masson staining of liver tissue and the degree of liver fibrosis in each group. Results are expressed as mean±standard deviation (SD), n=6. ** P<0.01, *** P<0.001, and **** P<0.0001: compared with CG; ## P<0.01: MG compared with TG; ns: no significant difference. LBPs: *Lycium barbarum* polysaccharides; CCl₄: carbon tetrachloride; ALT: alanine aminotransferase; AST: aspartate aminotransferase; H&E: hematoxylin and eosin; CG: control group; MG: model group; TG: treatment group.

of mitochondria in the TG was increased, the nucleus and nucleolus were relatively normal, mitochondria were normal in morphology and structure, but the density of mitochondria in the TG was still lower than that in the CG.

The level of liver fibrosis in each experimental group is shown in Figs. 1d and 1e. The liver in MG had extensive fibrosis, a high collagen fiber area ratio, and damage to the hepatic cable structure. The degree of fibrosis in the TG was much lower than that in the MG, while the collagen fiber area ratio was nevertheless larger than that in the CG.

3.2 Improvement of the antioxidant capacity of the liver by regulating the p62-Keap1-Nrf2 pathway with LBPs

The *p62*, *Keap1*, and *Nrf2* gene transcription levels in the MG were lower than those in the CG (Fig. 2a). In contrast to the MG, the expression of the *p62* and *Nrf2* genes in the TG was clearly enhanced, whereas the downward trend of *Keap1* was consistent with that of the MG. Additionally, there was no discernible difference between the MG and CG in terms of the expression of the protein p62 or Keap1, but
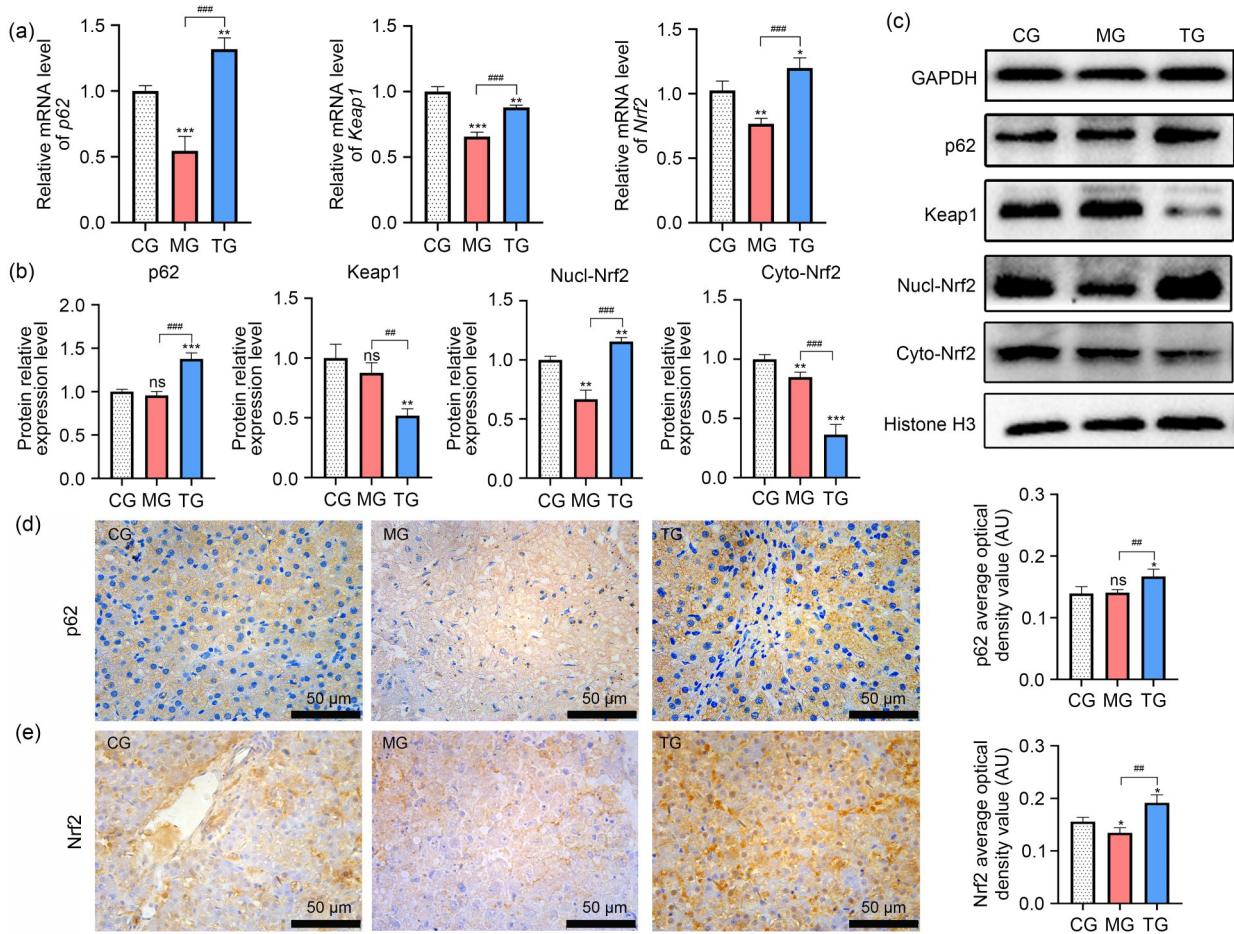
Fig. 2 Effect of LBPs on the p62-Keap1-Nrf2 pathway. (a) The mRNA expression levels of *p62*, *Keap1*, and *Nrf2*. (b, c) The protein expression levels of p62, Keap1, and Nucl/Cyto-Nrf2. (d) The immunohistochemical results of p62. (e) The immunohistochemical results of Nrf2. Results are expressed as mean±standard deviation (SD), *n*=6. * *P*<0.05, ** *P*< 0.01, and * *P*<0.001: compared with CG; ## *P*<0.01 and ### *P*<0.001: MG compared with TG; ns: no significant difference. LBPs: *Lycium barbarum* polysaccharides; mRNA: messenger RNA; GAPDH: glyceraldehyde-3-phosphate dehydrogenase; *p62*: sequestosome 1; *Keap1*: Kelch-like epichlorohydrin-associated protein 1; *Nrf2*: nuclear factor erythroid 2-related factor 2; Nucl: nucleus; Cyto: cytoplasm; AU: arbitrary unit; CG: control group; MG: model group; TG: treatment group.**

there was a clear down-regulation of Nrf2 in both the nucleus and the cytoplasm in the MG. In contrast to the MG and CG, Keap1 and cytoplasmic Nrf2 (Cyto-Nrf2) protein expression levels showed a significant negative trend, while p62 and nuclear Nrf2 (Nucl-Nrf2) in the TG were noticeably up-regulated (Figs. 2b and 2c). The immunohistochemistry analysis of p62 revealed no discernible differences between the MG and CG, except that the TG had a much greater positive expression rate of p62 than that in the CG (Fig. 2d). According to the Nrf2 immunohistochemistry findings, the Nrf2-positive signal was weaker in the MG than in the CG, and the brown signal was primarily found in the cytoplasm, indicating that most Nrf2 did not enter the nucleus, whereas there were a lot of brown and yellow Nrf2-positive signals in the TG liver nucleus, and significantly more than those in the CG (Fig. 2e).

3.3 Promotion of the expression of downstream antioxidant genes and proteins of Nrf2 by LBPs for reduction of oxidative damage

SOD1, SOD2, Trx1, Trx2, HO-1, CAT, GR, GPX1, GPX4, G6PD, and PRDX3 have been confirmed to be transcriptional sites of Nrf2 and regulated by Nrf2 (Myers, 2012; Shelton and Jaiswal, 2013; Raghunath et al., 2018; Tu et al., 2019; Gou et al., 2020). Fig. 3 illustrates how LBPs affect the expression of downstream antioxidant genes and proteins. According to the findings, all antioxidant genes
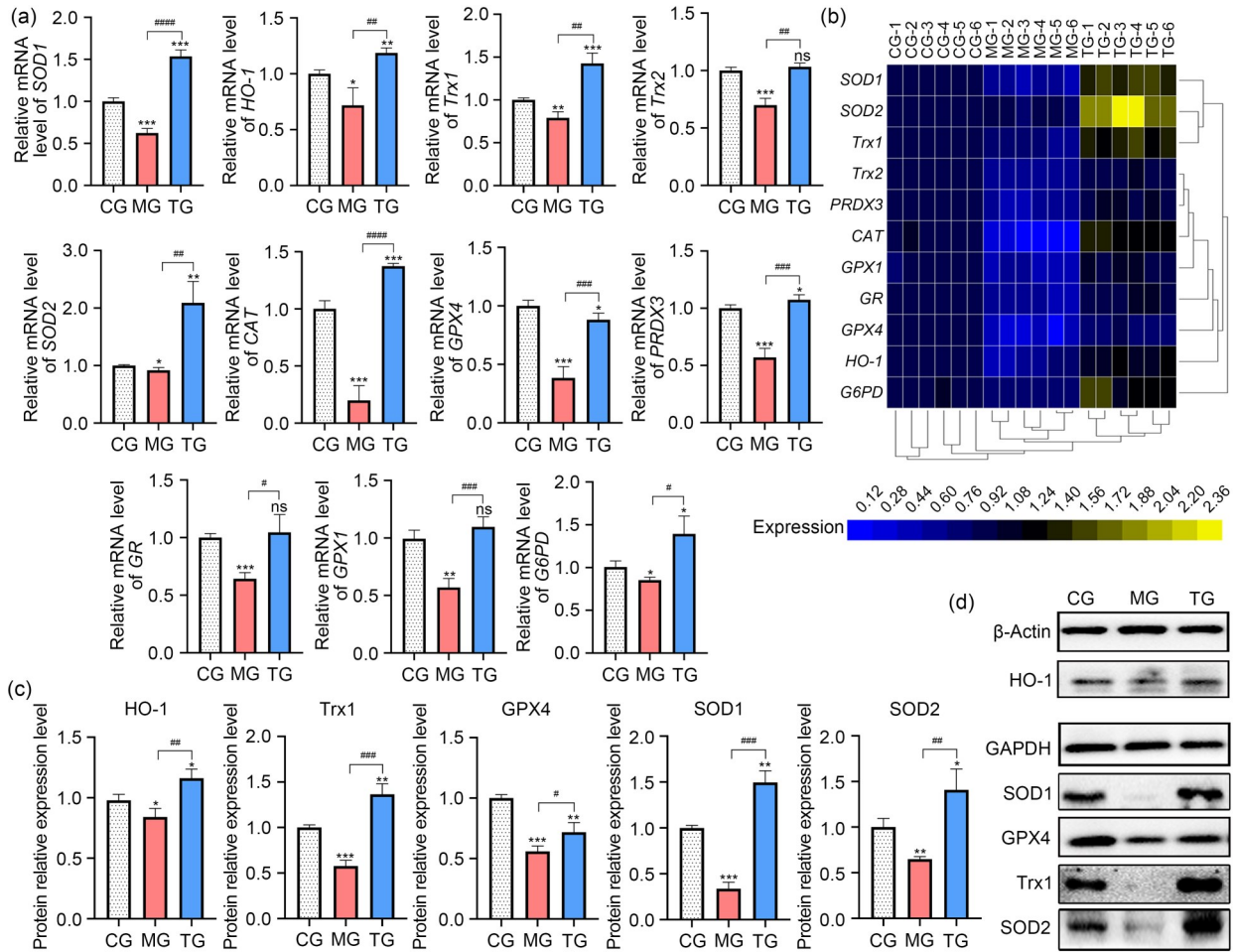
Fig. 3 Effects of LBPs on downstream antioxidant genes and proteins of Nrf2. (a) The mRNA expression levels of related antioxidant genes regulated by ARE. (b) Differences in the expression of related antioxidant genes regulated by ARE shown visually by a hierarchical clustering heat map. (c, d) The protein expression levels of HO-1, SOD1, GPX4, Trx1, and SOD2 detected by the western blot method. Results are expressed as mean±standard deviation (SD), n=6. * P<0.05, ** P<0.01, and *** P<0.001: compared with the CG; # P<0.05, ## P<0.01, ### P<0.001, and #### P<0.0001: MG compared with TG; ns: no significant difference. LBPs: *Lycium barbarum* **polysaccharides; mRNA: messenger RNA; Nrf2: nuclear factor erythroid 2-related factor 2; ARE: antioxidant response element; HO-1: heme oxygenase-1; GAPDH: glyceraldehyde-3-phosphate dehydrogenase; SOD1: superoxide dismutase 1; GPX4: glutathione peroxidase 4; Trx1: thioredoxin 1; CAT: catalase; GR: glutathione reductase; G6PD: glucose-6-phosphate dehydrogenase; PRDX3: peroxiredoxin 3; CG: control group; MG: model group; TG: treatment group.**

found in the MG had lower expression levels than those in the CG. However, the expression of genes *SOD1*, *HO-1*, *Trx1*, *SOD2*, *CAT*, *PRDX3*, and *G6PD* increased evidently in the TG, but the expression of the genes *GPX4*, *Trx2*, *GR*, and *GPX1* was restored to normal levels (Fig. 3a). The information on expression levels of these genes was gathered to create a hierarchical clustering heat map, which more clearly illustrates the inhibition of protective genes by acute liver injury and the repair and promotion of protective genes by LBPs (Fig. 3b). Protein expression analysis revealed that SOD1, SOD2, Trx1, GPX4, and HO-1

expression levels in the MG were lower than those in the CG. GPX4 expression was higher in the TG than in the MG, but was still only at a low level (Figs. 3c and 3d).

3.4 Reduction of oxidative damage by repairing or increasing the activity of antioxidant enzymes and increasing the reserve of reduction equivalent with LBPs

Except for CAT activity, the results demonstrated that the antioxidant enzyme activity in the MG was decreased to variable degrees compared to that in the CG, but the CAT results also suggested that not all

of the antioxidant systems in the MG had collapsed. The results of the TG showed that LBPs could successfully increase the enzyme activity of G6PD, CAT, and SOD1, and repair the enzyme activity of GR, GPX, and SOD2. However, TrxR activity had a limited potential to be saved (Fig. 4a). The GSH contents of the MG and TG were decreased while that of the TG was still much higher than that of the MG (Fig. 4a).

Cytochrome P450 family 2 subfamily E member 1 (CYP2E1) is an efficient generator of ROS. The MG had a considerably greater level of *CYP2E1* gene

expression than did the CG and TG (Fig. 4b). 8-OHDG is widely used as a biomarker of DNA oxidative damage. The level of 8-OHDG in the MG was clearly higher than that in the CG, suggesting that the DNA oxidative damage was more serious. The amount of 8-OHDG in the TG was much lower than that in the MG, while still being greater than that in the CG. The findings revealed that both the MG and TG had greater H_2O_2 content than the CG, although the H_2O_2 concentration in the TG was much lower than that in the MG (Fig. 4c). The MDA level in the MG was substantially
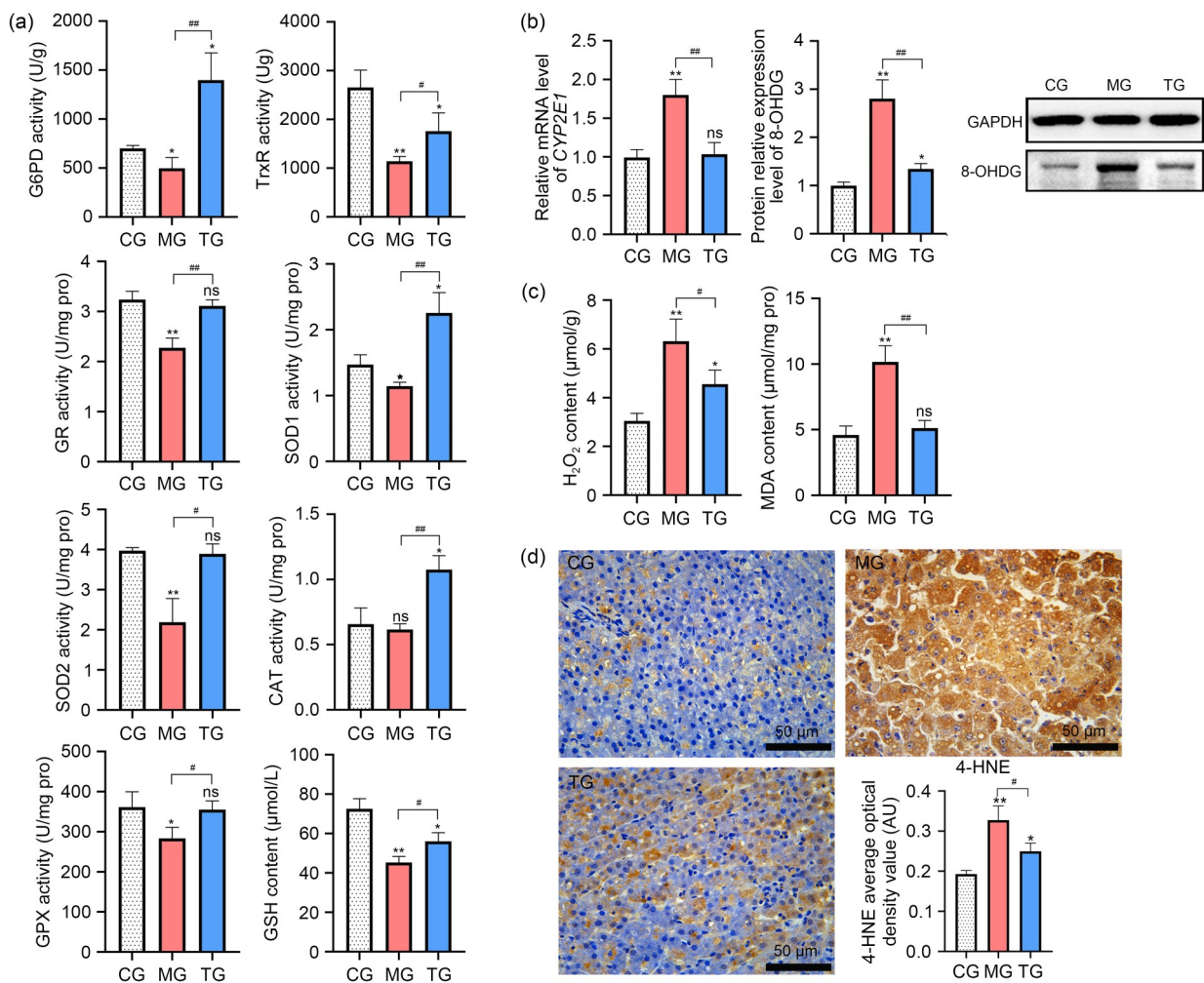

Fig. 4 Effects of LBPs on antioxidant oxidase activity, reductive equivalent, and oxidative damage identification indexes. (a) The activity of G6PD, TrxR, GR, SOD1, SOD2, CAT, and GPX, and the content of GSH. (b) The mRNA expression level of *CYP2E1* and the expression level of 8-OHDG. (c) Contents of MDA and H_2O_2. (d) The immunohistochemical results of 4-HNE. Results are expressed as mean±standard deviation (SD), n=6. * $P<0.05$ and ** $P<0.01$: compared with the CG; # $P<0.05$ and ## $P<0.01$: MG compared with TG; ns: no significant difference. LBPs: *Lycium barbarum* polysaccharides; mRNA: messenger RNA; G6PD: glucose-6-phosphate dehydrogenase; SOD: superoxide dismutase; CAT: catalase; TrxR: thioredoxin reductase; GPX: glutathione peroxidase; GR: glutathione reductase; GSH: glutathione; CYP2E1: cytochrome P450 family 2 subfamily E member 1; GAPDH: glyceraldehyde-3-phosphate dehydrogenase; pro: protein; 8-OHDG: 8-hydroxy-2-deoxyguanosine; MDA: malondialdehyde; H_2O_2: hydrogen peroxide; 4-HNE: 4-hydroxynonenal; AU: arbitrary unit; CG: control group; MG: model group; TG: treatment group.

greater than that in the CG, indicating that the lipid peroxidation of liver tissue had undergone significant modification (Fig. 4c). A biomarker for oxidative/nitrosative stress is 4-HNE. The brownish-yellow signal of 4-HNE protein expression in the MG was substantially greater than that in the CG and TG. The expression signal of 4-HNE in the TG was much lower than that in the MG, despite the brownish-yellow signal still being greater than that in the CG (Fig. 4d).

3.5 Improvement of the respiratory function of damaged mitochondria and increase of the content of tissue ATP by LBPs

The oxygen consumption rate (OCR, also known as the respiratory rate or oxygen flux) as it relates to

complex I is shown in Fig. 5a. The overall OCR of the MG was obviously lower than that of the CG. Compared with the CG, the routine respiration, spare respiratory capacity, maximal respiration, and respiratory control ratio of the MG were impaired, while in the TG, the routine respiration and mitochondrial respiratory control ratio were restored to the normal level. The maximal respiration and spare respiratory capacity had not completely recovered, but had improved (Fig. 5b).

The results of ATP revealed that the OXPHOS process of the MG was compromised and that its ATP content was reduced, whereas the ATP content of the TG appeared to have increased and exceeded that of the CG (Fig. 5a). The consumption of mitochondrial respiratory substrates (nicotinamide adenine dinucleotide
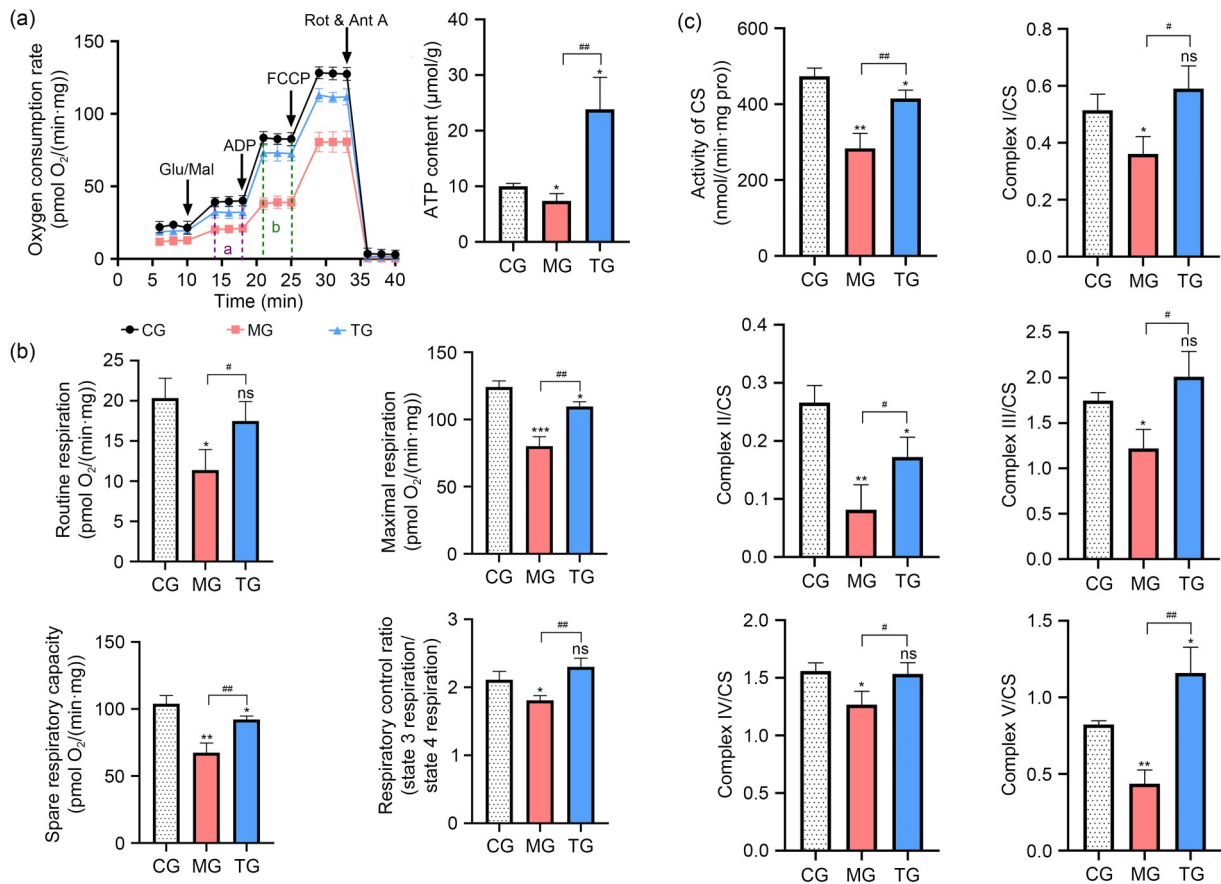

Fig. 5 Effect of LBPs on the function of mitochondrial respiration. (a) Mitochondrial respiratory rate measured by respirometer and tissue ATP content. a: state 4 respiration; b: state 3 respiration. FCCP: carbonyl cyanide 4-trifluoromethoxy-phenylhydrazone; ADP: adenosine diphosphate; Glu: glutamic acid; Mal: malic acid; Rot: rotenone; Ant A: antimycin A. (b) Mitochondrial routine respiration, spare respiratory capacity, maximal respiration, and respiratory control ratio were calculated by adding different substrates and inhibitors. (c) CS activity and ratio of activity of complexes I–V to activity of CS. Results are expressed as mean±standard deviation (SD), *n*=6. * *P*<0.05, ** *P*<0.01, and * *P*<0.001: compared with the CG; # *P*<0.05 and ## *P*<0.01: MG compared with TG; ns: no significant difference. LBPs: *Lycium barbarum* polysaccharides; ATP: adenosine triphosphate; O₂: oxygen; CS: citrate synthase; pro: protein; CG: control group; MG: model group; TG: treatment group.**

(NADH) and flavine adenine dinucleotide, reduced (FADH2)) and the effectiveness of electron transport are represented by the activity of the respiratory chain complex. Compared with the CG, the CS and complexes I–V activity of the MG was damaged to variable degrees, and tricarboxylic acid cycle and proton transport were disturbed. In the interim, complexes I, III, and IV activity matched those of the CG, and complex V activity was even enhanced, with the exception of CS and complex II activity, which did not recover to the usual level in the TG. However, CS and complex II activity was still much better than those of the MG (Fig. 5c).

3.6 Active regulation of the metabolic pathways of acute liver injury canines by LBPs

A total of 141 different metabolites that were enriched by MetbraAnalyst 5.0 were tested. A total of 10 metabolic pathways were involved in the process of liver injury caused by CCl_4 and the therapeutic action of LBPs, according to a path enrichment analysis (Fig. 6a). Glycerophospholipid metabolism, linoleic acid metabolism, α-linolenic acid metabolism, glycosylphosphatidylinositol (GPI)-anchor biosynthesis, and arachidonic acid metabolism were the five metabolic pathways with the greatest pathway effect value. The cluster heat map was created by MetbraAnalyst 5.0

using the first 38 metabolites with the greatest variable important in projection (VIP) value ($P<0.05$). The findings demonstrated that these metabolites significantly varied amongst the three experimental groups (Fig. 6b). The expression levels of the metabolites in the TG and MG were compared to those of the CG, and the $\log_2$(fold change) value for each metabolite was then calculated. After that, the 12 metabolites with the biggest variation in expression between the TG and MG were chosen (Table 1). The findings demonstrated that eight metabolite levels declined in the TG but increased in the MG most significantly, whereas four increased in the TG but reduced in the MG to a greater extent.

4 Discussion

Although numerous hepatoprotective medications have been researched and used in clinical settings, some may have negative side effects (Liu et al., 2014). Finding "liver protecting agents" that are efficient and safe for both animals and humans is thus important.

According to the findings of the experiments, LBPs can prevent oxidative damage by decreasing the expression of Keap1, increasing the expression of p62, and activating Nrf2. The increased expression levels
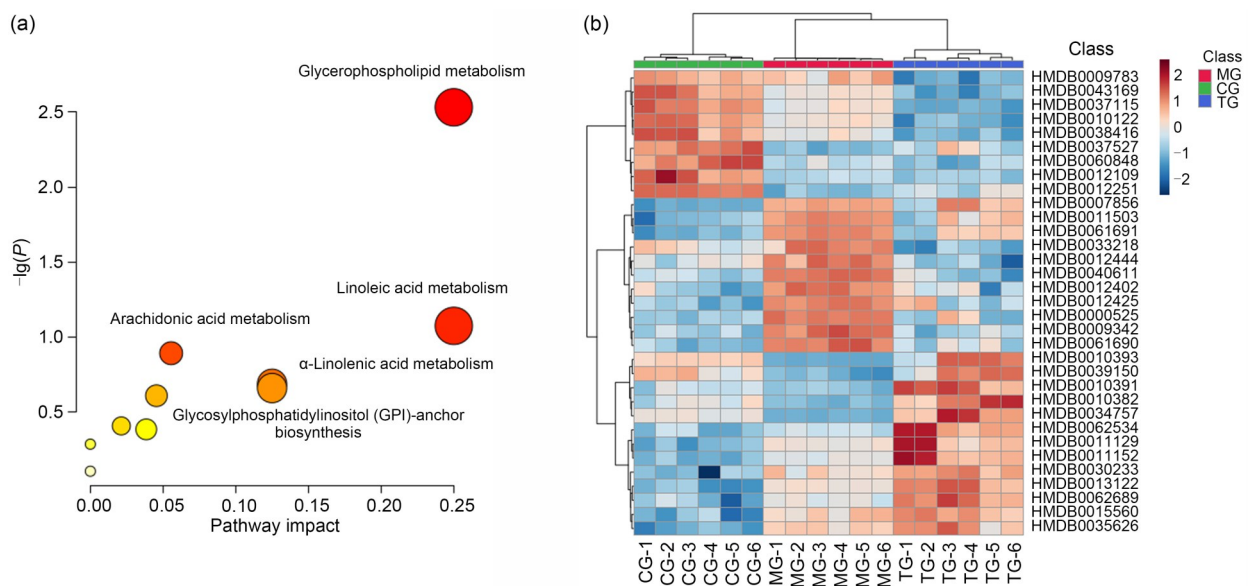

Fig. 6 Main metabolic pathways and metabolites regulated by LBPs in the treatment of acute liver injury. (a) Pathway analysis of the main differential metabolites in the liver. (b) A cluster heat map of the first 38 differential metabolites in the liver; red and blue represent the up-regulation and down-regulation of metabolites, respectively. LBPs: *Lycium barbarum* **polysaccharides; CG: control group; MG: model group; TG: treatment group; HMDB: the Human Metabolome Database.**

Table 1 First 12 metabolites with the most different expression in the MG and TG compared with the CG

HMDB ID	Metabolite	$\log_2$(fold change)	
		MG	TG
HMDB0034757	4-Methoxybenzene propanol 1-(2-sulfoglucoside)	−1.749 465 525	2.063 044 499
HMDB0010402	LysoPC (22:5 (4Z, 7Z, 10Z, 13Z, 16Z))	−1.872 372 824	1.770 261 707
HMDB0061883	Caproate (6:0)	−1.972 595 645	1.349 482 079
HMDB0010393	LysoPC (20:3 (5Z, 8Z, 11Z))	−1.648 135 217	1.085 991 362
HMDB0042040	Tipredane	1.327 642 219	−1.113 751 673
HMDB0009185	PE (18:4 (6Z, 9Z, 12Z, 15Z)/14:1 (9Z))	1.224 684 429	−2.182 379 043
HMDB0032844	4,5-Dihydroniveusin A	1.249 274 922	−2.531 588 018
HMDB0009181	PE (18:3 (9Z, 12Z, 15Z)/P-18:0)	1.856 621 306	−2.619 365 474
HMDB0010223	9-HODE	1.335 135 457	−2.812 219 681
HMDB0030767	11,12-Dimethoxydihydrokawain	2.319 154 115	−2.999 131 712
HMDB0002429	(3a,5b)-24-Oxo-24-[(2-sulfoethyl)amino]cholan-3-yl-b-D-glucopyranosiduronic acid	3.639 143 103	−3.053 959 516
HMDB0038158	Jangomolide	1.399 493 203	−3.095 003 637

HMDB: the Human Metabolome Database; ID: identity; CG: control group; MG: model group; TG: treatment group; LysoPC: lysophosphatidylcholine; PE: phosphatidylethanolamine; 9-HODE: 9-hydroxyoctadecadienoic acid.

of p62 and Nucl-Nrf2 represent an increase in cell survival rate (Lewis et al., 2015; Haga et al., 2017), which may be one of the key mechanisms by which LBPs lessen hepatocyte damage and boost hepatocyte lifespan.

Some antioxidant genes, such as *Trx1*, *GPX2*, and nicotinamide adenine dinucleotide phosphate (NAD(P)H):quinone oxidoreductase 1 (*NQO1*), are highly dependent on the regulation of Nrf2 (Xu et al., 2019). As a result, these antioxidant genes and proteins in the TG were expressed at levels higher than those of the CG due to the increased expression of Nrf2. Even while certain antioxidant genes were upregulated following LBP treatment, they were still suppressed compared to those in the CG. This may be because these genes are either not sensitive to Nrf2 or are only partially dependent on Nrf2, and are controlled by other genes.

The main reaction substrate for GPX4 is GSH. Toxic peroxides may be converted by GPX4 into non-toxic hydroxyl compounds using two equivalents of GSH (Liu WW et al., 2021). To counter the ongoing creation of harmful peroxides, many of the GPX4 proteins that have been translated interact with GSH. This may explain the regular expression of the *GPX4* gene, but reduced protein expression in the TG, as well as the decrease in GSH concentration. According to the relevant research, Nrf2-mediated genes must control liver functions such as GSH synthesis, binding, detoxification, and transport (Ma, 2010; Chen et al., 2020). If Nrf2 transcriptional activity decreases, GSH production will be lost (Jin et al., 2019). Therefore, the

partial recovery of GSH stores in the TG may be connected to Nrf2 activation by LBPs.

SOD2, PRDX3, and Trx2 regulated by Nrf2 are specifically located in mitochondria (Sun et al., 2015; Gao et al., 2018; Hu et al., 2018). After activation by mitochondrial deacetylase sirtuin 3 (Sirt3), SOD2 converts locally produced free radicals into H_2O_2 (Sharma et al., 2020), while Trx2 can provide electrons for PRDX3 to scavenge H_2O_2 from SOD2 conversion (Chen et al., 2019). Therefore, part of the reason for the decrease of H_2O_2 content in the TG compared with that in the MG may be that LBPs stimulate the expression of *SOD2*, *PRDX3*, and *Trx2* genes through Nrf2, while one of the important reasons for the high H_2O_2 content in the TG may be that LBPs did not fully restore the activity of TrxR. Therefore, through restoring and boosting Nrf2 expression in injured hepatocytes, LBPs are expected to partially repair mitochondrial redox equilibrium.

The reduction of routine respiration corresponds to a decrease in cell quantity (Kandel et al., 2016). The finding of H&E staining in the MG indicated that a significant number of damaged hepatocytes help to corroborate this theory. Although LBPs still partially repaired this damaged feature, the spare respiratory capacity of both the TG and MG was compromised, indicating that both groups of hepatocytes were less able to handle the abrupt rise in ATP demand. The decline in maximum respiratory rate is a significant sign of possible mitochondrial malfunction (Brand and Nicholls, 2011). Although symptoms in the TG were

less severe, the reduction in maximum respiratory rates of the MG and TG suggested that mitochondrial malfunction existed. The respiratory control ratio represents the efficiency of OXPHOS of mitochondria. The findings demonstrated that LBPs may effectively repair the OXPHOS system of mitochondria. OXPHOS is closely related to the formation of ATP. When the respiratory control ratio of the TG was not significantly enhanced, the ATP level of the TG was increased, and the enhanced activity of ATP synthase may be the reason for this phenomenon. The rise in ATP levels demonstrated the increased energy need of TG hepatocytes. We speculate that LBPs raise the ATP level to provide hepatocytes more energy to cope with their own damage. The activity of CS is regarded as a significant biomarker that reflects the density of mitochondria (Larsen et al., 2012), and the results of electron microscopic observation correspond to the results of CS activity. Ralph et al. (2011) made the observation that the functional impairment of complex II might lead to the production of ROS and the accumulation of succinate in cells. We thus hypothesize that the imbalance in redox homeostasis of the MG and TG may be caused by the impairment of the activity of complex II (such as a result of the increase in H_2O_2 content).

The outcomes of pathway enrichment demonstrated the critical role that lipid metabolism plays in the management of CCl_4-induced acute liver injury by LBPs. The results of this experiment were congruent with serum metabolomics research on liver injury, which found that serum lysophosphatidylcholine (LysoPC/LPC) was reduced in the liver injury group (Ma et al., 2014). The cause of the drop-in serum LPC levels is unknown. According to the study by Hinkovska-Galcheva et al. (2021), several medications can suppress lysosomal enzymes like phospholipase A2, which causes phospholipids to build up in lysosomes. At the same time, the secretion of LPC from the liver is quantitatively important for plasma LPC levels (Balogun et al., 2013). Therefore, some scholars suggested that the inhibition of hepatic phospholipase A2 might result in a decrease in the levels of LPC in the plasma (Saito et al., 2014), which may be the cause of the decrease of serum LPC observed in the MG. Phosphatidylethanolamine (PE) is a fundamental component of mammalian biological membranes and is involved in a multitude of cell physiological functions

(Vance, 2015). PE can also trigger OXPHOS (Calzada et al., 2019), which is crucial for the healthy operation of mitochondria. In disease processes, exposure to PE has been used as a biomarker of cell death (Elvas et al., 2017). PE is exposed and released into the blood when a significant number of hepatocytes die, leading to an increase of PE in the blood of the MG, which is compatible with the concept put forward in the research by Gonzalez et al. (2012). A ligand for the G protein-coupled receptor G2A (GPR132), 9-hydroxyoctadecadienoic acid (9-HODE), is a cyclooxygenase product of linoleic acid (Osthues et al., 2020). Under oxidative stress, 9-HODE produces and activates G2A through a non-enzymatic reaction, which activates the mitogen-activated protein kinase (MAPK) pathway and mediates intracellular calcium mobilization to promote the inflammatory process (Rolin et al., 2013). The level of serum 9-HODE dramatically rises during the time of liver fibrosis and inflammation caused by illness, according to previous research that has established a positive association between the concentrations of 9-HODE in the liver and serum (Maciejewska et al., 2020). Therefore, the high levels of oxidative stress, inflammation, and potential liver fibrosis may be indicated by the elevated 9-HODE in the MG. The study by Zhang et al. (2021) indicated that G2A functions as a proton-sensing G protein-coupled receptor, while LPC is an antagonist for this receptor that controls such proton-dependent G2A activation.

The therapeutic mechanism of LBPs on acute liver injury may be as follows: relieving the inhibition of hepatic phospholipase A2, increasing the LPC level, inhibiting G2A, and reducing the 9-HODE level, thereby reducing the level of inflammation and oxidative stress in liver tissue, intervening in cell death pathways such as iron death or apoptosis, lowering hepatocyte mortality, promoting the entry of PE in blood into the liver as raw materials for hepatocyte and mitochondrial regeneration, and then ultimately reducing liver injury. Three metabolites are undoubtedly candidates for use as blood indicators of acute liver injury.

This study validated the protective effect of LBPs on the liver and revealed the therapeutic mechanism of LBPs on acute liver injury. However, note that the treatment of liver injury by LBPs is not comprehensive. To enhance the therapeutic effects, LBP therapy of acute liver injury patients should be supplemented with medications targeting mitochondria (such as

mitoquinone (MitoQ)) or other hepatoprotective agents (such as glucuronolactone). There were some short-comings in our study: we did not set up an LBP control group and could not exclude some positive or negative effects of LBPs on the body of healthy canines. We will continue to conduct LBP-related experiments in canines to gain more insight into the effects of LBPs on the organism.

5 Conclusions

Overall, the therapeutic effect of LBPs on acute liver injury was supported: LBPs can eliminate excessive oxidants through the p62-Keap1-Nrf2 pathway, reduce oxidative damage, and improve the dysfunction of mitochondria. Lipid metabolism is the primary metabolic pathway involved in both the development of acute liver injury and the therapeutic role of LBPs. Additionally, three key possible biomarkers are LPC, PE, and 9-HODE. LBPs are therefore an effective option for the treatment of acute liver injury.

Author contributions

Jianjia HUANG: data curation, investigation, visualization, conceptualization, and writing original draft. Yuman BAI: formal analysis, investigation, and methodology. Wenting XIE: review and data curation. Rongmei WANG: funding acquisition. Wenyue QIU: investigation and conceptualization. Shuilian ZHOU: formal analysis. Zhaoxin TANG: resources. Jianzhao LIAO: writing, reviewing, and editing. Rongsheng SU: project administration, data curation, resources, supervision, writing, reviewing, and editing. All authors have read and approved the final manuscript, and therefore, have full access to all the data in the study and take responsibility for the integrity and security of the data.

Compliance with ethics guidelines

Jianjia HUANG, Yuman BAI, Wenting XIE, Rongmei WANG, Wenyue QIU, Shuilian ZHOU, Zhaoxin TANG, Jianzhao LIAO, and Rongsheng SU declare that they have no conflict of interest.

All institutional and national guidelines for the care and use of laboratory animals were followed. All experimental procedures and animal care were carried out in accordance with pertinent guidelines and regulations approved by the Institutional Animal Care and Use Committee of South China Agricultural University (No. 2020A132).

References

Balogun KA, Albert CJ, Ford DA, et al., 2013. Dietary omega-3 polyunsaturated fatty acids alter the fatty acid composition of hepatic and plasma bioactive lipids in C57BL/6 mice: a lipidomic approach. *PLoS ONE*, 8(11):e82399. https://doi.org/10.1371/journal.pone.0082399

Bellezza I, Giambanco I, Minelli A, et al., 2018. Nrf2-Keap1 signaling in oxidative and reductive stress. *Biochim Biophys Acta Mol Cell Res*, 1865(5):721-733. https://doi.org/10.1016/j.bbamcr.2018.02.010

Brand MD, Nicholls DG, 2011. Assessing mitochondrial dysfunction in cells. *Biochem J*, 435(2):297-312. https://doi.org/10.1042/BJ20110162

Caldez MJ, van Hul N, Koh HWL, et al., 2018. Metabolic remodeling during liver regeneration. *Dev Cell*, 47(4):425-438.e5. https://doi.org/10.1016/j.devcel.2018.09.020

Calzada E, Avery E, Sam PN, et al., 2019. Phosphatidylethanolamine made in the inner mitochondrial membrane is essential for yeast cytochrome bc_1 complex function. *Nat Commun*, 10:1432. https://doi.org/10.1038/s41467-019-09425-1

Chen CF, Wang K, Zhang HF, et al., 2019. A unique SUMO-interacting motif of Trx2 is critical for its mitochondrial presequence processing and anti-oxidant activity. *Front Physiol*, 10:1089. https://doi.org/10.3389/fphys.2019.01089

Chen YP, Liu KH, Zhang JW, et al., 2020. c-Jun NH_2-terminal protein kinase phosphorylates the Nrf2-ECH homology 6 domain of nuclear factor erythroid 2-related factor 2 and downregulates cytoprotective genes in acetaminophen-induced liver injury in mice. *Hepatology*, 71(5):1787-1801. https://doi.org/10.1002/hep.31116

Du X, Zhang JJ, Liu L, et al., 2022. A novel anticancer property of *Lycium barbarum* polysaccharide in triggering ferroptosis of breast cancer cells. *J Zhejiang Univ-Sci B (Biomed & Biotechnol)*, 23(4):286-299. https://doi.org/10.1631/jzus.B2100748

Elvas F, Stroobants S, Wyffels L, 2017. Phosphatidylethanolamine targeting for cell death imaging in early treatment response evaluation and disease diagnosis. *Apoptosis*, 22(8):971-987. https://doi.org/10.1007/s10495-017-1384-0

Frazier AE, Vincent AE, Turnbull DM, et al., 2020. Assessment of mitochondrial respiratory chain enzymes in cells and tissues. *Methods Cell Biol*, 155:121-156. https://doi.org/10.1016/bs.mcb.2019.11.007

Gao J, Feng ZH, Wang XQ, et al., 2018. SIRT3/SOD2 maintains

osteoblast differentiation and bone formation by regulating mitochondrial stress. *Cell Death Differ*, 25(2):229-240.
https://doi.org/10.1038/cdd.2017.144

Gonzalez E, van Liempd S, Conde-Vancells J, et al., 2012. Serum UPLC-MS/MS metabolic profiling in an experimental model for acute-liver injury reveals potential biomarkers for hepatotoxicity. *Metabolomics*, 8(6):997-1011.
https://doi.org/10.1007/s11306-011-0329-9

Gou ZX, Su XJ, Hu X, et al., 2020. Melatonin improves hypoxic-ischemic brain damage through the Akt/Nrf2/Gpx4 signaling pathway. *Brain Res Bull*, 163:40-48.
https://doi.org/10.1016/j.brainresbull.2020.07.011

Guo Q, Zhang QQ, Chen JQ, et al., 2017. Liver metabolomics study reveals protective function of *Phyllanthus urinaria* against CCl_4-induced liver injury. *Chin J Nat Med*, 15(7): 525-533.
https://doi.org/10.1016/S1875-5364(17)30078-X

Haga S, Yimin, Ozaki M, 2017. Relevance of FXR-p62/SQSTM1 pathway for survival and protection of mouse hepatocytes and liver, especially with steatosis. *BMC Gastroenterol*, 17:9.
https://doi.org/10.1186/s12876-016-0568-3

Hinkovska-Galcheva V, Treadwell T, Shillingford JM, et al., 2021. Inhibition of lysosomal phospholipase A2 predicts drug-induced phospholipidosis. *J Lipid Res*, 62:100089.
https://doi.org/10.1016/j.jlr.2021.100089

Hu W, Dang XB, Wang G, et al., 2018. Peroxiredoxin-3 attenuates traumatic neuronal injury through preservation of mitochondrial function. *Neurochem Int*, 114:120-126.
https://doi.org/10.1016/j.neuint.2018.02.004

Jain A, Lamark T, Sjøttem E, et al., 2010. *p62/SQSTM1* is a target gene for transcription factor NRF2 and creates a positive feedback loop by inducing antioxidant response element-driven gene transcription. *J Biol Chem*, 285(29): 22576-22591.
https://doi.org/10.1074/jbc.M110.118976

Jia R, Li Y, Cao LP, et al., 2019. Antioxidative, anti-inflammatory and hepatoprotective effects of resveratrol on oxidative stress-induced liver damage in tilapia (*Oreochromis niloticus*). *Comp Biochem Physiol C Toxicol Pharmacol*, 215: 56-66.
https://doi.org/10.1016/j.cbpc.2018.10.002

Jardim FR, de Almeida FJS, Luckachaki MD, et al., 2020. Effects of sulforaphane on brain mitochondria: mechanistic view and future directions. *J Zhejiang Univ-Sci B (Biomed & Biotechnol)*, 21(4):263-279.
https://doi.org/10.1631/jzus.B1900614

Jin Y, Huang ZL, Li L, et al., 2019. Quercetin attenuates toosendanin-induced hepatotoxicity through inducing the Nrf2/GCL/GSH antioxidant signaling pathway. *Acta Pharmacol Sin*, 40:75-85.
https://doi.org/10.1038/s41401-018-0024-8

Johnson CH, Ivanisevic J, Siuzdak G, 2016. Metabolomics: beyond biomarkers and towards mechanisms. *Nat Rev Mol Cell Biol*, 17(7):451-459.
https://doi.org/10.1038/nrm.2016.25

Kandel J, Angelin AA, Wallace DC, et al., 2016. Mitochondrial respiration is sensitive to cytoarchitectural breakdown. *Integr Biol (Camb)*, 8(11):1170-1182.
https://doi.org/10.1039/c6ib00192k

Larsen S, Nielsen J, Hansen CN, et al., 2012. Biomarkers of mitochondrial content in skeletal muscle of healthy young human subjects. *J Physiol*, 590(14):3349-3360.
https://doi.org/10.1113/jphysiol.2012.230185

Lewis KN, Wason E, Edrey YH, et al., 2015. Regulation of Nrf2 signaling and longevity in naturally long-lived rodents. *Proc Natl Acad Sci USA*, 112(12):3722-3727.
https://doi.org/10.1073/pnas.1417566112

Lin SY, Xu D, Du XX, et al., 2019. Protective effects of salidroside against carbon tetrachloride (CCl_4)-induced liver injury by initiating mitochondria to resist oxidative stress in mice. *Int J Mol Sci*, 20(13):3187.
https://doi.org/10.3390/ijms20133187

Liu BX, Zeng QW, Chen HM, et al., 2021. The hepatotoxicity of altrazine exposure in mice involves the intestinal microbiota. *Chemosphere*, 272:129572.
https://doi.org/10.1016/j.chemosphere.2021.129572

Liu JZ, Wang X, Liu R, et al., 2014. Oleanolic acid co-administration alleviates ethanol-induced hepatic injury via Nrf-2 and ethanol-metabolizing modulating in rats. *Chem Biol Interact*, 221:88-98.
https://doi.org/10.1016/j.cbi.2014.07.017

Liu WW, Zhou Y, Duan WZ, et al., 2021. Glutathione peroxidase 4-dependent glutathione high-consumption drives acquired platinum chemoresistance in lung cancer-derived brain metastasis. *Clin Transl Med*, 11(9):e517.
https://doi.org/10.1002/ctm2.517

Lustgarten MS, Bhattacharya A, Muller FL, et al., 2012. Complex I generated, mitochondrial matrix-directed superoxide is released from the mitochondria through voltage dependent anion channels. *Biochem Biophys Res Commun*, 422(3):515-521.
https://doi.org/10.1016/j.bbrc.2012.05.055

Ma J, Yu J, Su XR, et al., 2014. UPLC-MS-based serum metabonomics for identifying acute liver injury biomarkers in Chinese miniature pigs. *Toxicol Lett*, 225(3):358-366.
https://doi.org/10.1016/j.toxlet.2014.01.008

Ma Q, 2010. Transcriptional responses to oxidative stress: pathological and toxicological implications. *Pharmacol Ther*, 125(3):376-393.
https://doi.org/10.1016/j.pharmthera.2009.11.004

Maciejewska D, Drozd A, Skonieczna-Żydecka K, et al., 2020. Eicosanoids in nonalcoholic fatty liver disease (NAFLD) progression. Do serum eicosanoids profile correspond with liver eicosanoids content during NAFLD development and progression? *Molecules*, 25(9):2026.
https://doi.org/10.3390/molecules25092026

Myers CR, 2012. The effects of chromium (VI) on the thioredoxin system: implications for redox regulation. *Free

Radic Biol Med, 52(10):2091-2107.
https://doi.org/10.1016/j.freeradbiomed.2012.03.013

Osthues T, Zimmer B, Rimola V, et al., 2020. The lipid receptor G2A (GPR132) mediates macrophage migration in nerve injury-induced neuropathic pain. *Cells*, 9(7):1740.
https://doi.org/10.3390/cells9071740

Qiao N, Yang YY, Liao JZ, et al., 2021. Metabolomics and transcriptomics indicated the molecular targets of copper to the pig kidney. *Ecotoxicol Environ Saf*, 218:112284.
https://doi.org/10.1016/j.ecoenv.2021.112284

Raghunath A, Sundarraj K, Nagarajan R, et al., 2018. Antioxidant response elements: discovery, classes, regulation and potential applications. *Redox Biol*, 17:297-314.
https://doi.org/10.1016/j.redox.2018.05.002

Ralph SJ, Moreno-Sánchez R, Neuzil J, et al., 2011. Inhibitors of succinate: quinone reductase/Complex II regulate production of mitochondrial reactive oxygen species and protect normal cells from ischemic damage but induce specific cancer cell death. *Pharm Res*, 28(11):2695-2730.
https://doi.org/10.1007/s11095-011-0566-7

Rolin J, Al-Jaderi Z, Maghazachi AA, 2013. Oxidized lipids and lysophosphatidylcholine induce the chemotaxis and intracellular calcium influx in natural killer cells. *Immunobiology*, 218(6):875-883.
https://doi.org/10.1016/j.imbio.2012.10.009

Saito K, Maekawa K, Ishikawa M, et al., 2014. Glucosylceramide and lysophosphatidylcholines as potential blood biomarkers for drug-induced hepatic phospholipidosis. *Toxicol Sci*, 141(2):377-386.
https://doi.org/10.1093/toxsci/kfu132

Sharma S, Bhattarai S, Ara H, et al., 2020. SOD2 deficiency in cardiomyocytes defines defective mitochondrial bioenergetics as a cause of lethal dilated cardiomyopathy. *Redox Biol*, 37:101740.
https://doi.org/10.1016/j.redox.2020.101740

Shelton P, Jaiswal AK, 2013. The transcription factor NF-E2-related factor 2 (Nrf2): a protooncogene? *FASEB J*, 27(2):414-423.
https://doi.org/10.1096/fj.12-217257

Sun HY, Hu YJ, Zhao XY, et al., 2015. Age-related changes in mitochondrial antioxidant enzyme Trx2 and TXNIP–Trx2–ASK1 signal pathways in the auditory cortex of a mimetic aging rat model: changes to Trx2 in the auditory cortex. *FEBS J*, 282(14):2758-2774.
https://doi.org/10.1111/febs.13324

Tian XJ, Liang TS, Liu YL, et al., 2019. Extraction, structural characterization, and biological functions of *Lycium barbarum* polysaccharides: a review. *Biomolecules*, 9(9):389.
https://doi.org/10.3390/biom9090389

Tu WJ, Wang H, Li S, et al., 2019. The anti-inflammatory and anti-oxidant mechanisms of the Keap1/Nrf2/ARE signaling pathway in chronic diseases. *Aging Dis*, 10(3):637-651.
https://doi.org/10.14336/AD.2018.0513

Vance JE, 2015. Phospholipid synthesis and transport in mammalian cells. *Traffic*, 16(1):1-18.
https://doi.org/10.1111/tra.12230

Venâncio C, Antunes L, Félix L, et al., 2013. Chronic ketamine administration impairs mitochondrial complex I in the rat liver. *Life Sci*, 93(12-14):464-470.
https://doi.org/10.1016/j.lfs.2013.08.001

Wang M, Wang L, Han L, et al., 2017. The effect of carabrone on mitochondrial respiratory chain complexes in *Gaeumannomyces graminis*. *J Appl Microbiol*, 123(5):1100-1110.
https://doi.org/10.1111/jam.13554

Wu ZG, Han MF, Chen T, et al., 2010. Acute liver failure: mechanisms of immune-mediated liver injury. *Liver Int*, 30(6):782-794.
https://doi.org/10.1111/j.1478-3231.2010.02262.x

Xin YF, Zhang S, Gu LQ, et al., 2011. Electrocardiographic and biochemical evidence for the cardioprotective effect of antioxidants in acute doxorubicin-induced cardiotoxicity in the beagle dogs. *Biol Pharm Bull*, 34(10):1523-1526.
https://doi.org/10.1248/bpb.34.1523

Xu DW, Xu M, Jeong S, et al., 2019. The role of Nrf2 in liver disease: novel molecular mechanisms and therapeutic approaches. *Front Pharmacol*, 9:1428.
https://doi.org/10.3389/fphar.2018.01428

Zhang JQ, Shi L, Xu XN, et al., 2014. Therapeutic detoxification of quercetin against carbon tetrachloride-induced acute liver injury in mice and its mechanism. *J Zhejiang Univ-Sci B (Biomed & Biotechnol)*, 15(12):1039-1047.
https://doi.org/10.1631/jzus.B1400104

Zhang Q, Zhang W, Liu J, et al., 2021. Lysophosphatidylcholine promotes intercellular adhesion molecule-1 and vascular cell adhesion molecule-1 expression in human umbilical vein endothelial cells via an orphan G protein receptor 2-mediated signaling pathway. *Bioengineered*, 12(1):4520-4535.
https://doi.org/10.1080/21655979.2021.1956671

Zhao YN, Lu J, Mao AK, et al., 2021. Autophagy inhibition plays a protective role in ferroptosis induced by alcohol via the p62–Keap1–Nrf2 pathway. *J Agric Food Chem*, 69(33):9671-9683.
https://doi.org/10.1021/acs.jafc.1c03751

Supplementary information

Table S1; Figs. S1–S7; Materials and methods